Cement and Concrete Research 42 (2012) 74–83

Contents lists available at SciVerse ScienceDirect

Cement and Concrete Research

journal homepage: http://ees.elsevier.com/CEMCON/default.asp

Influence of slag chemistry on the hydration of alkali-activated blast-furnace slag — Part II: Effect of Al_2O_3

M. Ben Haha, B. Lothenbach *, G. Le Saout, F. Winnefeld

Empa, Swiss Federal Laboratories for Materials Science and Technology, Laboratory for Concrete and Construction Chemistry, Ueberlandstrasse 129, 8600 Dübendorf, Switzerland

ARTICLE INFO

Article history:
Received 8 April 2011
Accepted 16 August 2011

Keywords:
Alkali activated slags (D)
Al_2O_3 content (D)
Hydration (A)
Microstructure (B)
Hydrotalcite (D)

ABSTRACT

The hydration and microstructural evolution of three alkali activated slags (AAS) with Al_2O_3 contents between 7 and 17% wt.% have been investigated. The slags were hydrated in the presence of two different alkaline activators, NaOH and $Na_2SiO_3 \cdot 5H_2O$. The formation of C(−A)–S–H and hydrotalcite was observed in all samples by X-ray diffraction, thermal analysis and scanning electron microscopy. Higher Al_2O_3 content of the slag decreased the Mg/Al ratio of hydrotalcite, increased the Al incorporation in the C(−A)-S-H and led to the formation of strätlingite. Increasing Al_2O_3 content of the slag slowed down the early hydration and a lower compressive strength during the first days was observed. At 28 days and longer, no significant effects of slag Al_2O_3 content on the degree of hydration, the volume of the hydrates, the coarse porosity or on the compressive strengths were observed.

1. Introduction

Alkali-activated binders based on ground granulated blast-furnace slag represent a viable and sustainable alternative to Portland cement since they use by-products of other industrial manufacturing processes. They often exhibit a rapid setting, fast strength development and high resistance to chemical attack [1–3]. Alkalis are used to stimulate the dissolution of the slag and thus the formation of hydration products, mainly calcium silicate hydrates incorporating significant amounts of aluminium, C(−A)-S-H, a hydrotalcite-like phase and strätlingite [4–9]. The reactivity of the slag depends mainly on the mineralogical composition, the fineness of the slag and on the type and concentration of the alkaline activator used.

A fundamental understanding of physical and chemical effects of the chemical compositions of the slags and of the effect of different activators on the hydration mechanisms can give a deeper insight into the relationship between composition and mechanical properties. A better understanding of the slag chemistry may lead to the development of more durable concretes and could indicate ways to use less reactive slags efficiently.

In a previous study it has been found that increasing MgO contents in alkali activated blast furnace slag slow down the early hydration but lead in the long-term to higher compressive strengths [10] as the formation of additional hydrotalcite leads to an increased volume of the solid and thus to a lower coarse porosity. The present study aims to investigate the effect of different Al_2O_3 contents in the slag on the kinetics of slag reaction and on compressive strength.

Experimental studies on the effect of Al_2O_3 on alkali activated slags are rare. Sakulich et al. [11] reported a delay of the hydration reaction in NaOH/waterglass activated slags which were mixed with high quantities of separately added Al_2O_3. They observed that the addition of a low amount of Al_2O_3 (2 wt.%) increased the 7 and 28 days compressive strength, whilst the addition of 15 wt.% or more did not further improve the mechanical properties.

A recent study on supersulphated slags activated by 15 wt.% $CaSO_4$ and 0.5 wt.% KOH showed that the slags containing more Al_2O_3 exhibited a higher reactivity during the first week and a corresponding higher strength [2]. After longer reaction times, the degree of hydration was found to be similar, but for the high Al_2O_3 slag a higher compressive strength was observed. Gruskovnjak ea. [2] related the higher compressive strength of the Al_2O_3 rich slag to the higher amount of voluminous ettringite formed and thus to a higher degree of space filling.

The present study aims to investigate the effect of Al_2O_3 in the slag on the hydration properties of alkali activated slag over 1 year, using three slags with different Al_2O_3 contents whilst the contents of the other oxides are nearly the same. The slags were activated by sodium metasilicate pentahydrate (waterglass: WG) and sodium hydroxide. The effect of the Al_2O_3 on strength, rate of hydration, and the nature of the different hydrates are investigated using calorimetry, thermogravimetry, X-ray diffraction, scanning electron microscopy and thermodynamic modelling.

* Corresponding author. Tel.: +41 58 765 47 88; fax: +41 58 765 823 40 35.
E-mail address: barbara.lothenbach@empa.ch (B. Lothenbach).

0008-8846/$ – see front matter © 2011 Elsevier Ltd. All rights reserved.
doi:10.1016/j.cemconres.2011.08.005

2. Materials and methods

2.1. Slags

The three granulated blastfurnace slags were ground in a laboratory ball mill to a specific surface of 5000 +/− 100 cm^2/g (Table 1).

2.2. Binder and paste formulation

Two alkaline activators, NaOH (3.77 g/100 g slag) and sodium water glass $Na_2SiO_3 \cdot 5H_2O$ (WG) (10.0 g/100 g slag) were used, resulting in the same Na_2O content in both cases and in the presence of an additional 2.8 SiO_2/100 g slag in the WG-activated systems. The alkaline activators were dissolved in the water prior the mixing. The water was added taking into account the crystal water of WG to insure a water to binder ratio of 0.40.

2.3. Methods

2.3.1. Anhydrous slags

The chemical composition of the anhydrous slags was analysed by XRF using a Philips PW 2400 instrument (Table 1). Their particle size distribution was determined with a laser granulometer Malvern Mastersizer X.

X-ray powder diffraction XRD was carried out with an incident beam monochromator and CuKα radiation (λ = 1.54 Å) on a PANalytical X'Pert Pro MPD diffractometer in θ–2θ configuration with an angular scan 5–65° 2θ and an X'Celerator detector. An internal standard (CaF_2) was added to the anhydrous slag in order to deduce the amount of amorphous [12].

The ^{29}Si MAS NMR spectra were recorded on a Bruker Avance 400 NMR spectrometer (field strength of 9.4 T) at 79.49 MHz applying 4.5 kHz spinning rates on a 7 mm CP MAS probe using ZrO_2 rotors. Single-pulse experiments were carried out by applying 90° pulses of 8.8 μs with ^1H decoupling of 31.3 kHz (TPPM15) and recycle delays of 4 s in order to respect the relaxation time T_1 of the species present in the samples (a T_1 of less than 1 s was determined for the slag by a T_1 saturation recovery experiment). The ^{29}Si chemical shift was referenced externally relative to tetramethylsilane at 0.0 ppm. The observed ^{29}Si resonances were analysed using the $Q^n(mAl)$ classification, where a Si tetrahedron is connected to n Si tetrahedra with n varying from 0 to 4; m is the number of neighbouring AlO_4 tetrahedra.

The ^{27}Al MAS NMR spectra were obtained at 104.26 MHz on a 2.5 mm CP MAS probe using the above mentioned NMR system. Single pulse experiments were carried out at 20 kHz spinning rates by applying single pulse (π/12) excitation pulses of 0.5 μs and 0.5 s relaxation delays. The ^{27}Al chemical shifts were referenced relative to a 1.0 M $AlCl_3 \cdot 6H_2O$ solution at 0.0 ppm.

Table 1
Chemical composition (g/100g) and granular properties of the slags used in the study.

	A7	A14	A17
SiO_2	41.6	38.2	37.2
Al_2O_3	7.0	14.1	16.7
Fe_2O_3[a]	1.3	1.4	1.4
CaO	39.1	36.0	35.0
MgO	7.2	6.6	6.4
SO_3	1.3	1.2	1.0
K_2O	0.6	0.6	0.5
Na_2O	0.5	0.5	0.5
TiO_2	0.3	0.3	0.2
Mn_2O_3	1.1	1.0	1.0
Molar Ca/Si	1.01	1.01	1.01
Molar Mg/Al	1.29	0.60	0.49
Density (g/cm^3)	2.90	2.88	2.87
Blaine (cm^2/g)	5021	4963	4985
% R63 μm	0.2	0.4	0.1
% R18 μm	21.6	22.4	22.4
% R3 μm	74.9	76.5	75.6

[a] Including iron form the laboratory milling.

2.3.2. Hydrated samples

About 5 g of paste (water/binder = 0.40) were mixed externally, filled in a glass vial and loaded in a TAM Air isothermal calorimeter in order to determine the rate of heat liberation during the first week of hydration at 20 °C. The heat flow was measured on duplicate samples, the difference between the two measurements was negligible. Prior to mixing, the unhydrated slag, the water and the activator were equilibrated to the measurement temperature for at least 16 h. In a separate experiment, about 2.5 g of paste were mixed internally using the admix ampoule in order to follow the early hydration of the slags.

All paste samples were cured in sealed plastic container at 20 °C. The compressive strengths were determined on duplicate pastes samples using two cubes 25 × 25 × 25 mm per testing age. The pastes were demolded and cut into cubes prior to testing.

For XRD and TGA measurements, the hydration of the paste samples was stopped by solvent exchange with isopropanol. Before analyses, the samples were grinded by hand below 63 μm. TGA was performed between 30 and 980 °C at a heat rate of 20 K/min in a Mettler Toledo TGA/SDTA851. The amount of bound water was determined from the weight loss between 30 and 650 °C. Triplicate measurements of several samples indicated that the measurement inaccuracy for total bound water was ±0.2 g/100 g. XRD was performed as described above, but without CaF_2 standard, on one sample for each measurement time.

Slices of hydrated samples were cut, immediately immersed in isopropanol and subsequently dried at 40 °C for 24 h for the microscopical investigations. They were then impregnated using a low viscosity epoxy resin and polished down to ¼ μm. The samples were further coated with carbon and examined using a Philips ESEM FEG XL 30 scanning electron microscope (SEM). Backscattered electron images (BSE) were analysed quantitatively to determine the coarse porosity and the degree of reaction at different hydration times using image analysis (IA) [13–15]. The volume of coarser pores as determined by SEM-IA includes, depending on the magnification (2500×) used, pore sizes in the range of 0.05 to 5 μm and is referred to as "coarse porosity" in this paper. To be statistically representative, over 80 images were taken for each studied sample at a magnification of 2500. Energy dispersive X-ray spectroscopy (EDX) was applied to determine the elemental compositions of the hydrate assemblage and the different element ratio of the different hydrates. The analyses were carried out using an accelerating voltage of 15 kV to ensure a good compromise between spatial resolution and adequate excitation of the FeK_α peak.

2.3.3. Thermodynamic modelling

Thermodynamic calculations using the geochemical modelling code GEMS [16] were carried out using a consistent set of cement specific thermodynamic data, cemdata2007 [17,18], which had been originally compiled and verified for Portland cement systems. The cemdata2007 dataset includes thermodynamic data of common cement minerals such as C–S–H, different AFt and AFm phases, hydrotalcite and hydrogarnets [18]. No restrictions on the kind of hydrates calculated were imposed, with the exception of siliceous hydrogarnet ($C_3AS_{0.8}H_{4.4}$), whose formation was suppressed as its formation seems to be kinetically hindered at ambient temperatures [18]. The uptake of alkalis by C–S–H was approached by using an ideal solid solution model between jennite, tobermorite, $[(KOH)_{2.5} \cdot SiO_2 \cdot H_2O]_{0.2}$ and $[(NaOH)_{2.5} \cdot SiO_2 \cdot H_2O]_{0.2}$ as proposed by Kulik et al. [19]. The aluminium uptake in the C(−A)–S–H was taken into account based on the EDX measurements. It was assumed that the incorporation of aluminium, which occurs mainly at bridging sites [20,21], does not influence the molar volume of the C–S–H, as the incorporation of Al seems to stabilise the 14-Å tobermorite [22]. The kind and volume of solids precipitated were calculated using the density of the phases present in the sample. The initial composition

based on the XRF data (cf. Table 1) and the composition of the activator were used as input.

3. Analysis of the unhydrated slags

Varying Al_2O_3 contents may cause differences in the chemical and physical characteristics of the slags. Thus a detailed analysis of the three anhydrous slags is performed.

3.1. Chemical composition

The chemical compositions determined by X-ray fluorescence (XRF) and the granular properties of the three slags are given in Table 1. The Al_2O_3 contents of the slags are 7.0 wt.% (slag A7), 14.1 wt.% (slag A14) and 16.7 wt.-% (slag A17). The contents of the other oxides are comparable amongst the slags.

3.2. XRD

Rietveld analysis of the X-ray patterns of the slags shows only a minor contents of crystalline phases (Table 2). Akermanite occurs in the A7 slag and traces of anhydrite in all slags. The elemental iron has been introduced by the iron ball mill used in the grinding process.

Although the disorder of the amorphous phase in the different slags is certainly different, we observe a similar diffuse X-ray scattering present as a hump located around 0.3 nm ($2\theta = 30°$) for all slags (Fig. 1).

3.3. ^{29}Si and ^{27}Al NMR

^{29}Si and ^{27}Al NMR have been performed to observe the effect of higher Al_2O_3 content on the structure of the glasses (Fig. 2). The ^{29}Si NMR spectra reveal a broad signal centred around −74 ppm with a full width at half maximum of approximately 19 ppm. Similar chemical shifts are observed for akermanite and gehlenite (−73.7 and −72.5 ppm respectively [23]) which are the main constituents of crystalline phases that occur when the amorphous slag liquid is slowly quenched [24] or during devitrification [25]. By comparison with the crystalline phases, Shimoda et al. [24] conclude that the polymerisation structure around Si in the slag is on average close to chain-like linkage fashion, $Q^2(1Al)$ and $Q^2(2Al)$. The linewidth indicates the coexistence of Q^0 to Q^3 species with varying numbers of neighbouring AlO_4 tetrahedra. The ^{27}Al NMR spectra confirm that the aluminium is in fourfold coordination in slag as previously observed for blast furnace slags [24,25]. We observe little or no influence on the NMR spectra when the weight fraction of Al_2O_3 increases from 7 to 17 wt.% showing that the incorporation of Al^{3+} does not influence the distribution of Q^n species in the slag. However, as suggested by Shimoda et al. [26], it may influence the coordination number of Mg and Ca.

4. Results and discussion

4.1. Compressive strength

Activating the slags using NaOH results in relatively high early strength, whilst only a modest increase in compressive strength is observed for hydration times longer than 28 days. For a given age, no

Table 2
Phase composition of the slags by XRD (Rietveld analysis) in g/100 g.

	A7	A14	A17
Akermanite	3.1	0.0	0.0
Anhydrite	0.3	0.4	0.3
Amorphous	96.0	99.0	99.0
Iron	0.6	0.6	0.6

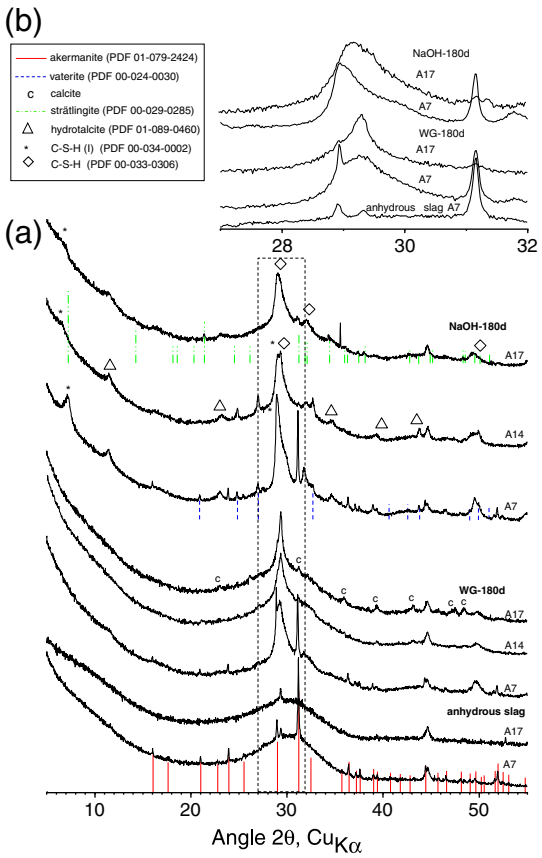

Fig. 1. XRD patterns of A7 and A17 slags anhydrous slags and comparison of the XRD patterns of the different WG and NaOH activated slags at 180 days.

significant difference in the compressive strength of the NaOH activated slag pastes containing different amounts of Al_2O_3 is observed (Table 3). The observation that the strength of NaOH activated pastes is not significantly affected by the chemical composition of the slag agrees with a previous study investigating the influence of MgO content [10].

Using the WG as activator, the hydration proceeds much slower than if NaOH is used but the compressive strengths of the paste samples continue to increase beyond 7 days; the samples gain 25 to 40% in compressive strength between 7 and 180 days. Increasing the Al_2O_3 content of the slags results in a slightly slower strength development at early ages, but similar compressive strengths are reached at late (28 days and longer) hydration times. The Al_2O_3 content of the slag is found to have no significant impact on the late compressive strength of the WG activated slags, in contrast to the MgO content which increased the compressive strength as reported previously [10].

The lower compressive strength after 7 days and longer of the NaOH activated systems compared to the WG activated slags agrees well with

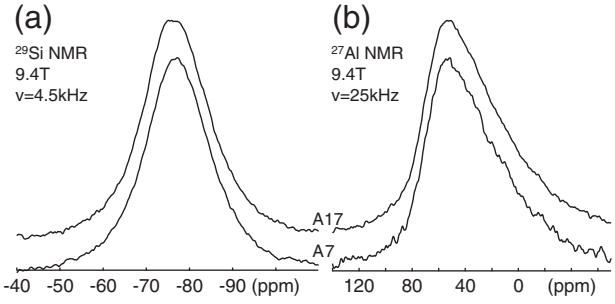

Fig. 2. (a) ^{29}Si and (b) ^{27}Al NMR spectra of the A7 and A17 slags.

Table 3
Compressive strengths of the slag pastes in MPa (±2 MPa).

	NaOH			WG		
	A7	A14	A17	A7	A14	A17
1 day	6.3	8.5	8.2	n.m.	n.m.	n.m.
7 days	12.3	13.7	14.3	36.7	31.5	32.9
28 days	19.1	21.3	23.3	39.5	37.7	37.5
90 days	23.2	24.7	27.5	44.2	43.5	43.2
180 days	25.2	25.7	26.3	46.2	45.2	45.1

n.m.: not measured due to poor strength.

findings reported in other studies [8,10,27–32]. The WG activated slags contain slightly more solids (2.8 g SiO_2/100 g slag) than the NaOH activated systems. This corresponds to 10 wt.% of the amount of slag reacted after 7 days and to 7 wt.% after 1 year (Table 4) and is thus expected to have a minor influence on the compressive strengths.

4.2. Hydration kinetics

4.2.1. Heat of hydration

The heat of hydration of alkali activated slags as a function of time is presented in Fig. 3 and the cumulative heat in Fig. 4. The general trends are in agreement with previous studies [10,33]. The hydration of the NaOH activated slag results in an initial peak during the first minutes (Fig. 3a, [33]) and a main peak between 1 and 24 h (Fig. 3b, [10,33]). The WG activated slags exhibit a relatively long dormant period of more than 60 h and the main reaction peak is observed only after 3 days (Fig. 3d). For the WG activated slags an initial peak in the first minutes is observed (Fig. 3c) and, in addition, a second early peak after 0.1 to 4 h as previously reported by Shi et al. [33]. They assigned the initial peak to the wetting and dissolution of the slag whereas the second early peak observed in the WG activated slag was assigned to the formation of "primary C–S–H".

In the NaOH activated slag, higher Al_2O_3 content of the slag accelerates the main peak between 1 and 24 h (Fig. 3b), as also mirrored in the cumulative heat reported in Fig. 4a during the first 2 days. However, after more than 2 days the slag A7 shows the highest and A17 the lowest cumulative heat as the reaction of A7 produces more heat after 1 day.

The slags activated by WG show a slight acceleration of the two initial peaks for A14 and A17 (Fig. 3c), but a clear delay of the main reaction peak with higher Al_2O_3 content (Fig. 3d). After 5 days, the cumulative heat is still slightly lower for A17 than for the A7 slag (Fig. 4b).

4.2.2. Slag dissolution

SEM image analysis is used to determine the degree of hydration by comparing the quantity of anhydrous slag left with the original volume of the slag in the paste or mortar [10,28,34]. The amount of slag reacted by SEM image analysis has been observed to give comparable results as by ^{29}Si NMR [35].

The initial reaction of NaOH activated slag is fast, whilst for the slags activated by WG only a hydration degree of 2–3% is reached after 1 day compared to 25% after 7 days (Table 4). This agrees with

Table 4
Degree of slag reaction measured by SEM-IA (weight percent ±3).

Activator	NaOH			WG		
Slag	A7	A14	A17	A7	A14	A17
1 day	18.1	17.4	16.9	n.m.	n.m.	n.m.
7 days	27.7	25.6	23.3	27.0	25.5	24.9
28 days	32.2	31.7	29.8	31.9	31.2	30.2
90 days	39.1	38.8	39.0	37.3	36.8	36.5
180 days	41.8	41.9	41.7	41.1	40.8	40.2
360 days	43.2	42.7	43.9	42.7	43.2	42.2

n.m.: not measured.

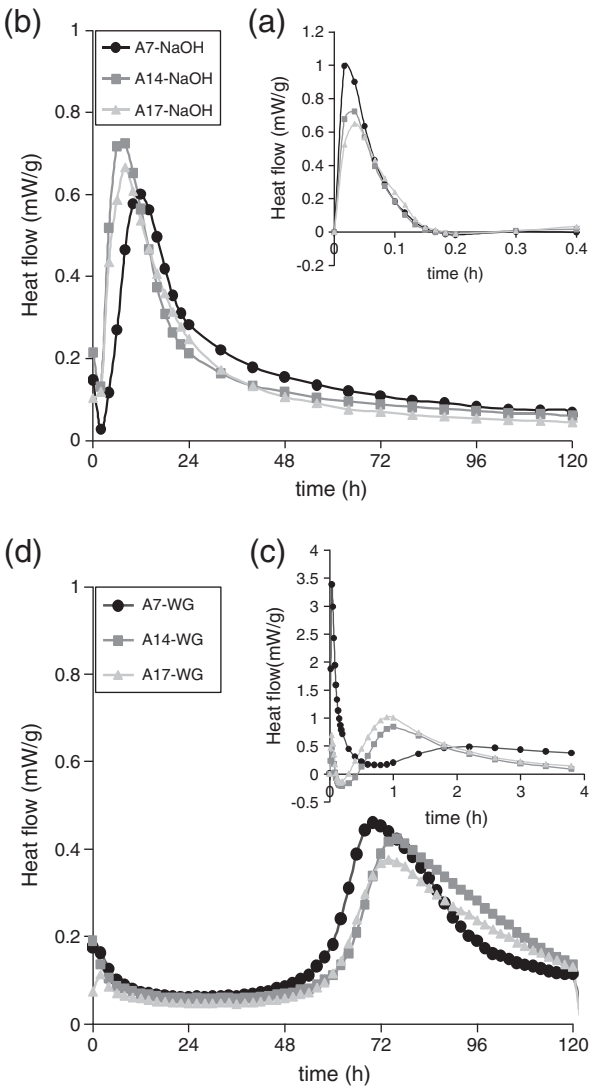

Fig. 3. Influence of the Al_2O_3 content of the slag on the hydration kinetics using NaOH (a) at early ages (internal mixing), (b) up to 5 days (external mixing), using WG (c) at early ages (internal mixing) and (d) up to 5 days (external mixing).

the delay in the main hydration peak for the WG slags during the first 2 days and the absence of measurable compressive strength after 1 day. After 28 days and longer, however, the observed reaction degrees are similar in all systems which is consistent with previous observations [10,28].

An increase of the Al_2O_3 content of the slag lowers slightly the degree of slag reaction for both NaOH and WG activated slags, most distinctly during the first 7 days (Table 4), which is consistent with calorimetry data (Figs. 3 and 4) where less total heat is observed after 5 days in the presence of more Al_2O_3. At later ages no significant differences are observed. The slightly lower degree of the early slag reaction is in contrast to the strength development (Table 3), where slightly higher early strengths are observed at higher Al_2O_3 contents. The differences, however, are relatively small and within the standard deviation of the strength measurements.

Two different effects could be responsible for the somewhat slower hydration during the first week for the higher Al_2O_3 content:

(i) The presence of more Al_2O_3 in the slag might influence its reactivity. It has been reported that a higher aluminium fraction in the silicate network of different minerals accelerated their dissolution strongly in acidic solutions [36,37]. This effect is strong at pH 3, but negligible at pH 6 [37]. No data are available at high

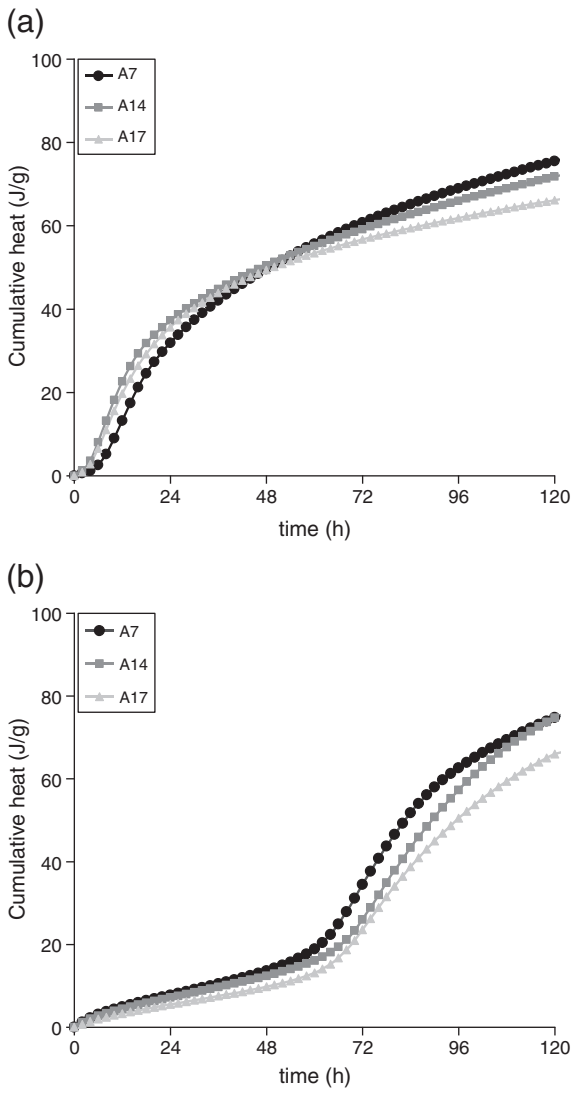

Fig. 4. Influence of the Al_2O_3 content of the slag on the cumulative heat of (a) NaOH and (b) WG activated slags during hydration (external mixing).

pH values which would be relevant for alkali activated slags, thus it is unclear whether the aluminium fraction in the solid has any influence on the reaction rate at high pH values. In addition, the NMR results in Fig. 2 show that the polymerisation of the silicates in the glass is not significantly influenced by the amount of Al_2O_3.

(ii) Also the dissolved aluminium concentrations could play an important role. It has been reported that the presence of dissolved aluminium (in millimolar concentrations) decreased drastically the dissolution rate of amorphous silica [38], basaltic glass [36,39] and quartz [40]. In the SiO_2 rich slags similar effects might be expected. The presence of more aluminium in the slag leads to more dissolved aluminium in the pore solution [41] as also mirrored in the higher aluminium content of the C–S–H (see Section 4.3.1 Hydrates below). Thus the observed delay of the hydration in alkali activated slags where Al_2O_3 has been added externally [11] and in the present study where the additional Al_2O_3 constitutes a part of the slag could be related to increased aluminium concentrations.

4.2.3. Bound water content

The bound water content as derived from the TGA analyses has been used as a measure of the hydration degree of a slag [30,34]. It has been observed, however, that the hydration products formed upon WG activation incorporate much more water than the NaOH activated slags [10,28,30], which makes the comparison between the two activators difficult.

The weight loss measurements in Table 5 show that the WG activates the slag more slowly than NaOH in agreement with calorimetric and image analysis results. For both activators, little additional water is bound in the hydrates after 28 days even though the slags continue to react slowly as observed by image analysis (Table 4) and as mirrored in the increase in compressive strength (Table 3). After 90 days and longer, the WG activated slags containing less Al_2O_3 show more bound water than A14 and A17. The difference is smaller for the NaOH activated slags. As at longer hydration times the same degree of slag dissolution is observed by image analysis (Table 4), this indicates the presence of hydrates which contain more water in the A7 than in the slags with higher Al_2O_3 content.

4.3. Hydrates

4.3.1. Solid phases

XRD shows the presence of C–S–H and a hydrotalcite like phase as already observed in other studies on hydrated alkali activated slags [3,4,6,9,10,17,28]. XRD analyses indicate also the presence of strätlingite for the A17 NaOH activated slag (Fig. 1). The hydration pattern is more complex for the NaOH than for the WG activated pastes. In addition to hydrotalcite and C–S–H, peaks corresponding to a second type of C–S–H, C–S–H (I), are detected (Fig. 1) as reported previously [10,28]. We can notice that the reflections of C–S–H (I) and hydrotalcite become broader with more Al_2O_3. The basal reflection of C–S–H (I) at 7° 2θ shifts toward a higher d spacing and is strongly broadened as the amount of aluminium increases from 7 wt.% to 14 wt.%. As proposed by Renaudin et al. [42], this may be explained by the insertion of aluminium in the C–S–H structure that leads to a decrease in the coherent domain.

The presence of C–S–H (main weight loss 50–200 °C) and of a hydrotalcite-like phase (weight loss at around 200 °C and 400 °C) [43,44] are confirmed by the TGA data (see Fig. 5). The weight losses indicate that much less hydrotalcite is formed than C–S–H.

EDX measurements indicate the presence of C–S–H containing aluminium and hydrotalcite. The Si, Mg, and Al contents were used to plot the Mg/Si vs. Al/Si ratios (Figs. 7 and 8) as described by Taylor et al. [3]. The good correlation of Mg/Si with Al/Si indicates the presence of a hydrotalcite-like phase, whilst the presence of a positive x-axis intercept reveals the level of Al incorporation in the C–S–H. Only a few points at 7 days indicate towards the possible presence of strätlingite in the A17 slag. The formation of AFm-type phases such as strätlingite has been reported in other studies [6,45].

Less C–S–H (or C–S–H with less water) is formed in the slags with high Al_2O_3 content as indicated by the derivative TGA data in Fig. 5 between 30 and 180 °C. It is not possible to quantify the amount of C–S–H as the weight loss of C–S–H, strätlingite and hydrotalcite overlap in this temperature range (Fig. 6, [34]). The average Ca/Si ratio of the C–S–H determined by SEM-EDX is approx. 0.8 in the case of WG activator and 0.9 for NaOH (Table 7). The slightly lower Ca/Si ratio in the WG activated slag is due to the presence of additional SiO_2 (2.8 g SiO_2/100 g slag) from the WG activator ($Na_2SiO_3 \cdot 5H_2O$). The Ca/Si ratios are

Table 5
Weight loss (±1 wt.%) between 30 °C and 650 °C determined by TGA of the hydrated samples (weight percent relative to the hydrated slag).

Activator	NaOH			WG		
Slag	A7	A14	A17	A7	A14	A17
1 day	7.9	9.2	9.6	7.3	7.0	6.2
7 days	11.2	10.3	9.6	11.7	13.1	12.2
28 days	10.5	11.0	11.0	14.1	13.4	12.5
90 days	11.2	11.0	10.8	14.5	13.3	12.5
180 days	11.9	11.0	10.8	14.9	13.4	12.4
360 days	12.2	11.5	11.1	15.2	13.2	12.4

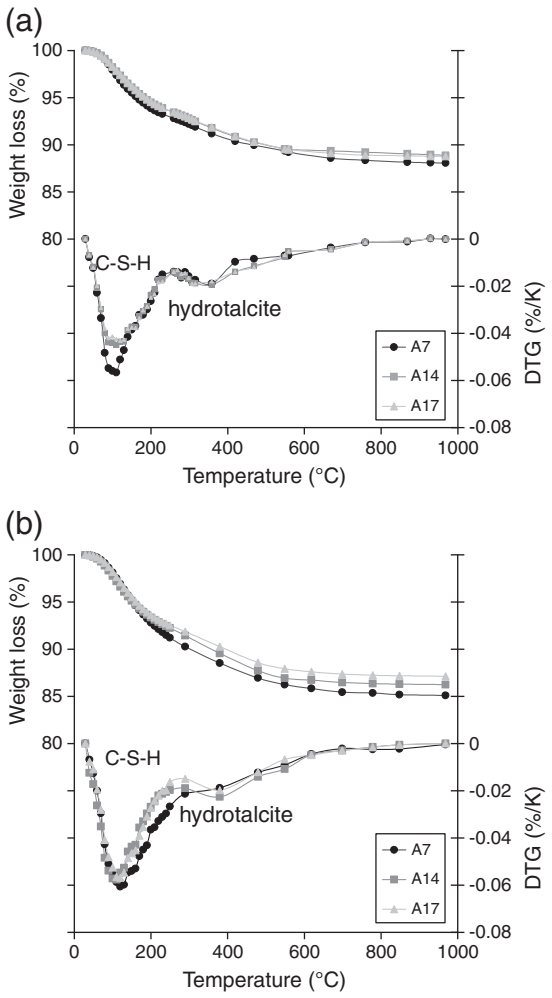

Fig. 5. Influence of the Al_2O_3 content of the slag on TGA and differential TGA (DTG) curves of the slags with (a) NaOH and (b) WG activation after a hydration time of 90 days.

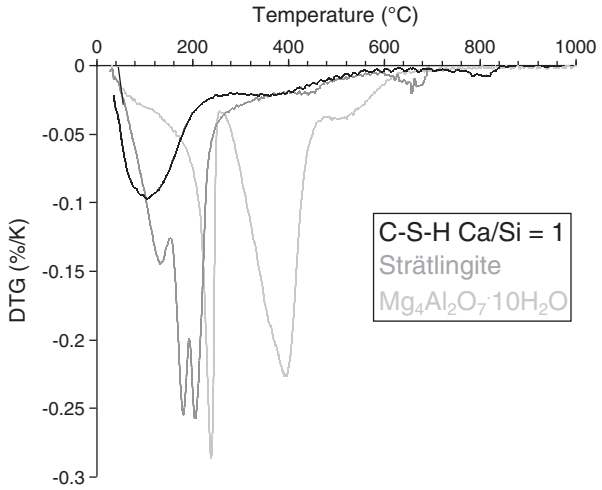

Fig. 6. Differential thermogravimetry (DTG) data of synthesised C–S–H, strätlingite and hydrotalcite; the main phases present in hydrated slag pastes.

influenced neither by the hydration time nor by the Al_2O_3 content of the slag (Table 7), as also reported in previous studies [10,28].

The C–S–H formed from slag hydration is generally richer in aluminium [46,47] than that formed in OPC or blended OPC systems. Higher Al_2O_3 contents in the slag increase the Al incorporation in the C–S–H (Table 7), as also visible in the increase of the abscissa on the Al/Si axis in Fig. 7 from 0.11 for A7 to 0.27 for A17. The highest observed value is near to the theoretically the maximum Al incorporation in the C–S–H of 0.33 [48], if all the bridging position of the dreierkette structure of the C–S–H are occupied by aluminium. However, possibly some Al can be also be inserted in the interlayer part of the C–S–H, resulting in even higher maximum Al incorporation as suggested by Renaudin et al. [42].

Also the composition of the hydrotalcite-like phase is affected by the different Al_2O_3 contents of the slag. The hydrotalcite-like phases formed during the first days have a Mg/Al ratio of approximately 2, which strongly decreases with time to a value as low as 1.3 for the slags A14 and A17 as shown in Figs. 7 and 8. A Mg/Al ratio of approximately 2 in the hydrotalcite-like phase is consistent with previous investigations [6,10,28,49] in alkali activated systems, where slags with Mg/Al from 0.8 to 1.5 in the unhydrated slag had been used. The lower Mg/Al ratio in the hydrotalcite observed for A14 and A17 (Table 7, Fig. 7) seems to be related to the very low Mg/Al ratio in the unhydrated slags (0.6 and 0.5, respectively, see Table 1). Synthetic hydrotalcite with Mg/Al ratios down to 0.5 have been reported [50]. For the higher Al_2O_3 content slags, a less well defined XRD peak (Fig. 1) but a similar "shoulder" of hydrotalcite in the TGA diagrams (Fig. 5) is observed at longer hydration times. This could be related to the formation of a hydrotalcite poorer in MgO at higher Al_2O_3 content, to a hydrotalcite-like solid with a poorer crystallinity or just to the slightly less MgO present in A14 and A17 (Table 1) resulting in the formation of less hydrotalcite.

Thus, the increase of Al_2O_3 content in slag results in an increased Al uptake in C–S–H, in the long-term in the formation of an Al-richer hydrotalcite-like phase and also in the presence of strätlingite.

4.3.2. Microstructure

During the first day of hydration the formation of hydrates around unhydrated slag particles is observed for the NaOH activated slags (Fig. 9). In contrast, no or little precipitation of hydrates is observed for the WG activated samples at that time. In the NaOH activated samples the formation of hydrotalcite platelets can be observed at early ages directly in the pore space (Fig. 9).

The samples activated by NaOH form rather narrow and dense hydration rims at the place of the reacted slag grains (Fig. 10). The dense hydrates, which develop very early in the NaOH activated slags, probably have a lower water content than the hydrates of WG-activated slag (see bound water contents in Table 5) as reported also previously [10,28]. These narrow hydration rims result in a coarse microstructure and relatively high coarse porosity as reported in Table 8. In the case of the WG

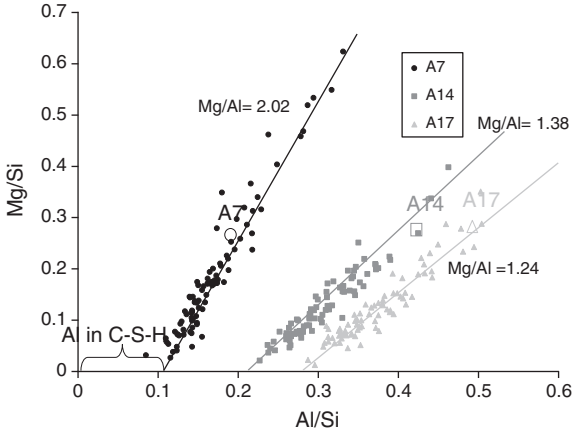

Fig. 7. Atomic Mg/Si versus Al/Si ratios of the WG activated slags after a hydration time of 180 days. The slope of the linear lines confirms the presence of a hydrotalcite-like phase with a Mg/Al of 1.2, 1.4 and 2.0. The intercept at 0.27, 0.21 and 0.11 in the Al/Si axis indicate that the C–S–H phases contain significant proportions of aluminium. The empty symbols indicate the molar ratios in the unhydrated slags.

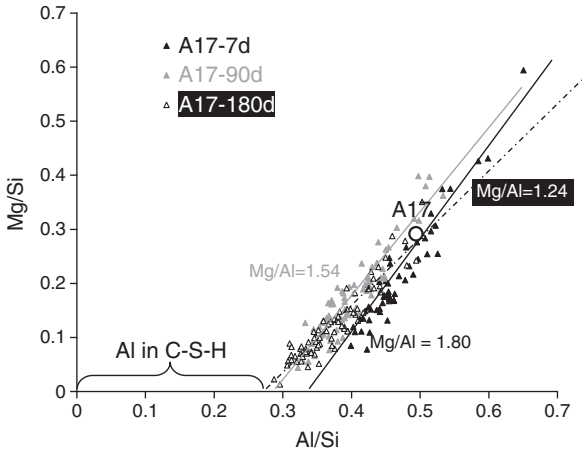

Fig. 8. Atomic Mg/Si versus Al/Si ratios of the WG activated A17 after different hydration times. The decrease in the slope from 1.8 to 1.2 indicates a decrease in the Mg/Al ratio of the hydrotalcite-like phase with time. The intercept of approx. 0.34, 0.29 and 0.27 in the Al/Si axis indicate that the C–S–H phases contain significant proportions of aluminium. The empty circle indicates the molar ratio in the unhydrated slag.

activated slags, the space is well filled by hydrates and almost no coarse pores are observed at longer hydration times (Fig. 10). A thin rim is found at the original boundary of the unhydrated slag grain.

No influence of the Al_2O_3 content on the microstructure is visible. All slags show comparable porosity and a comparable amount of anhydrous slag particles left up to 360 days (Table 4).

4.4. Thermodynamic modelling

The thermodynamic calculations predict the presence of C–S–H (Ca/Si ~1), hydrotalcite and ~1 wt.% of FeS. At higher Al_2O_3 contents also the formation of strätlingite ($2CaO \cdot Al_2O_3 \cdot SiO_2 \cdot 8H_2O$) is predicted as shown in Fig. 11 (the compositions of the main hydrates and their density are complied in Table 6). The thermodynamic calculations indicate that more than 90% of the alkalis present are taken up by the C–S–H phase. The calculated pH value of 13.6 agrees well with reported pH values in the range of 13.4 to 13.7 for comparable alkali activated slag systems [4,51,52]. The calculations indicate that approx. 30 g H_2O/100 g slag would be consumed for the complete reaction of slag with a small increase of bound water (±2 H_2O/100 g slag) with increasing Al_2O_3 content, whilst the TGA measurements indicated a slight decrease of the amount of bound water with higher Al_2O_3 content (Table 5). The calculation of bound water in these systems is associated with a considerable

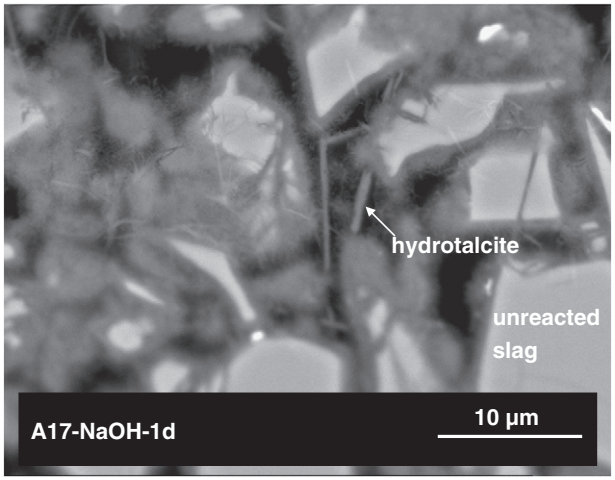

Fig. 9. SEM micrograph of NaOH activated A17 slag after 1 day showing the rim of hydrates around the slag particles and the presence of hydrotalcite platelets.

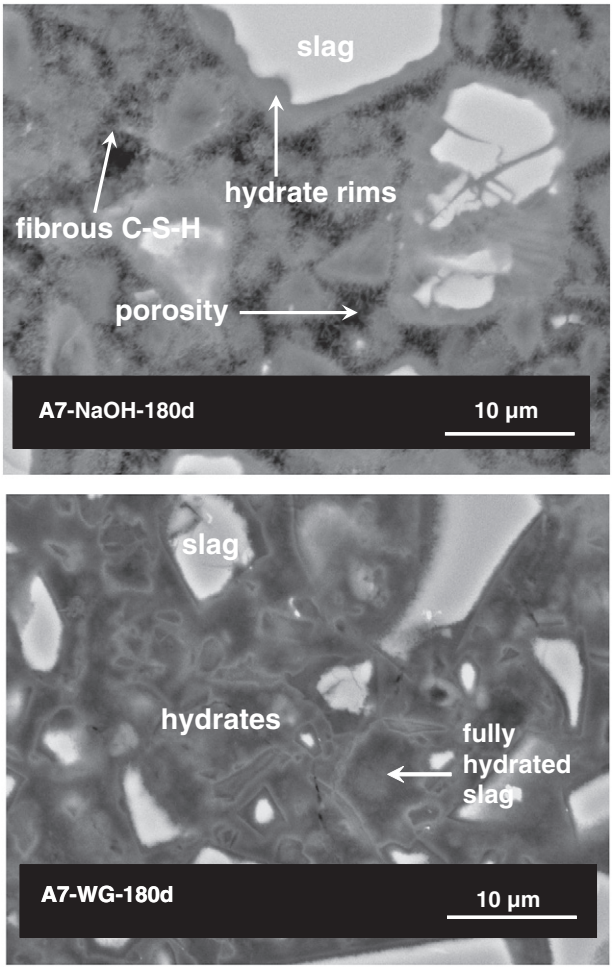

Fig. 10. SEM-micrographs of NaOH and WG activated A7 slag after 180 days. The bright hydrate rims observed in the NaOH activated samples indicate a relative higher density.

error as no quantitative information is available on the influence of alkalis and aluminium on the water content of C–S–H. However, the calculated water uptake of 30 g H_2O/100 g slag in the NaOH activated slag is compatible with the measured water loss of about 12 g/100 g at a reaction degree of the slag of 43% after 1 year (Table 5).

With increasing Al_2O_3 content in the slag, the total amount of C–S–H and hydrotalcite decreases, as the presence of more Al_2O_3 lowers the concentrations of CaO, SiO_2, MgO and other oxides present in the slag. The Al uptake by C–S–H and the Mg/Al ratio of the hydrotalcite have been considered based on the EDX measurements given in Table 7 and are indicated by the dotted lines in Fig. 11. The predicted phase assemblage is in good agreement with the experimental results where C–S–H, hydrotalcite-like phases as well as strätlingite for high Al_2O_3 content slags have been observed.

For both activators the same hydrate assemblage is calculated, with the only difference that a slightly lower Ca/Si ratio (Ca/Si = 0.9) in the C–S–H and 5% more C–S–H is calculated in the presence of WG compared to NaOH activated systems (Ca/Si = 1.0). This agrees well with the EDX measurements which indicate a lower Ca/Si ratio in the WG-activated slags. The calculations confirm the observation that the alkaline activator type has a minor influence on the composition of the hydrate assemblage.

At high Al_2O_3 content, the formation of strätlingite is predicted, which has been observed experimentally only for the A17 NaOH activated slags. The strätlingite is difficult to detect due to its poor crystallinity. At higher Al_2O_3 contents (>9%), where the formation of strätlingite is calculated, less C–S–H is calculated to be present, which

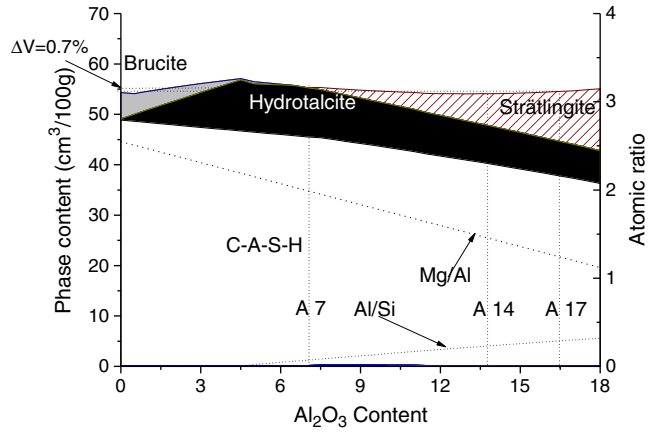

Fig. 11. Influence of Al_2O_3 content on the calculated volume of the hydrates present in NaOH activated slag. The dotted lines indicate the molar Al/Si in the C–S–H and Mg/Al ratio in hydrotalcite varied based on the EDX data. The difference in volume between hydrated slag A7 and A17 is indicated (ΔVol = 0.7%).

is consistent with the TGA data in Fig. 5. No relevant effect of the Al_2O_3 on the volume of the hydrates is predicted (Fig. 11) and thus no significant changes in the coarse porosity at the same degree of hydration are expected. The strätlingite (density 1.94 g/cm^3 [3,53]) formed at high Al_2O_3 content replaces partially hydrotalcite (2.03 g/cm^3 [54]), which results in little volume changes, and partially the denser tobermorite like C–S–H (2.23 g/cm^3 [55]), which should increase the total volume. However, at high Al_2O_3 content also more Al is incorporated in the bridging tetrahedra of the C–S–H, leading to less strätlingite and thus less volume. The effects compensate each other so that no significant volume changes are predicted. Whilst the amount of Al_2O_3 seems to have no significant influence on the volume of the hydrated alkali activated slags, the presence of additional MgO has been calculated to result in a clear increase of the volume of the hydrates and accordingly also in a higher compressive strength [10]. The presence of additional MgO led to less Al incorporation in C–S–H and to the formation of more voluminous hydrotalcite and thus to an increase in the degree of space filling.

5. Conclusions

The activation of slags using NaOH leads to a faster initial reaction and higher early compressive strength than observed for the water glass activated slags as reported also previously [10,28,32,56]. The fast reaction rate in the presence of NaOH leads to the formation of dense hydrate rims at the early stages of hydration, to a larger coarse porosity and thus a lower compressive strength at later ages compared with WG activated samples although comparable degrees of slag reaction are observed (Fig. 12a) at later ages as already discussed in detail previously [10,28].

The present paper focuses on the influence of the Al_2O_3 content on alkali activated blast furnace slags:

i) Higher Al_2O_3 content slows down slightly the rate of hydration during the first days for both NaOH and WG activated slags as indicated by the lower measured cumulative heat and the lower degree of slag reaction after 7 days. After 28 days and longer, a similar degree of reaction for both activators and all three slags was observed.
ii) The coarse porosity of the WG activated slags at 28 days and longer is very small and independent of the amount of Al_2O_3 present in the slag. In the slags activated by NaOH a much higher porosity at the same degree of reaction is observed in all slags, again independent of the amount of Al_2O_3.
iii) In the hydrated slags the presence of C–S–H (Ca/Si 0.8–0.9) and hydrotalcite is observed experimentally and also predicted by thermodynamic modelling. At high Al_2O_3 contents also the formation of strätlingite is observed.
iv) Higher Al_2O_3 content in the slag increases the Al incorporation in C–S–H in the hydrated pastes. Measured Al/Si ratios range from 0.11 (7% Al_2O_3) to 0.3 in the case of the slag with 17% Al_2O_3 content. A higher Al_2O_3 content in the slag increases also the quantity of Al_2O_3 in the hydrotalcite resulting in lower Mg/Al ratios of the hydrotalcite. Initially a hydrotalcite-like solid with Mg/Al of ~2 is formed, whilst at later ages lower Mg/Al ratios (1.3 for the 17% Al_2O_3 slag after 1 year) are observed indicating recrystallisation.
v) Thermodynamic calculations indicate that the Al_2O_3 content of the slag is not expected to have a significant influence on the volume of the hydrated samples, as the formation of strätlingite at high Al_2O_3 is compensated by the decrease of hydrotalcite, C–S–H and the increased Al-uptake in C–S–H (Fig. 11). The constant volume predicted by thermodynamic calculations agrees with the experimental observation that at longer hydration times the coarse porosity and the compressive strength of the paste samples are independent of the Al_2O_3 content (Table 3, Table 8, and Fig. 12).

In the present paper, the Al_2O_3 content of the alkali activated slags has found to change the composition of the hydrate assemblage but to not significantly influence the hydrate volume and the compressive strength. The presence of additional MgO, however, has been reported to decrease the porosity and to increase the compressive strength [10] as the presence of additional MgO leads to the formation of more hydrotalcite which has a lower density and thus a higher degree of space filling than C–S–H.

It should be noted that the effect of different Al_2O_3 or MgO content can depend strongly on the cementitious system studied. In supersulfated

Table 6
Theoretical and measured water content of C–S–H, strätlingite and hydrotalcite.

Phase	Formula	Theoretical water content (wt.%)	Measured weight loss (wt.%) (30–650 °C)	Density (g/cm^3)
Jennite like C–S–H, Ca/Si = 1.67	$Ca_{1.67}SiO_{3.67}$ 2.1H_2O	19.8	–	2.44 [58]
Tobermorite-like C–S–H, Ca/Si = 0.83	$Ca_{0.83}SiO_{2.83}$ 1.3H_2O	18.4	19.8 ± 1	2.23 [55]
Strätlingite	$Ca_2Al_2SiO_7$ 8H_2O	34.4	33.0 ± 1	1.94 [3,53]
Hydrotalcite	$Mg_4Al_2(OH)_{14}$ 3H_2O	40.6	44.1 ± 1	2.03 [54]

Table 7
Atomic ratios in the hydrate phases obtained by EDX analyses (±0.05).

Activator		NaOH			WG		
Slag	Age (days)	Ca/Si	Al/Si	Mg/Al	Ca/Si	Al/Si	Mg/Al
A7	7	0.89	0.11	2.06	0.74	0.10	1.97
	90	0.87	0.12	2.04	0.79	0.10	1.94
	180	0.88	0.12	2.02	0.79	0.11	2.02
	360	0.87	0.11	2.05	0.82	0.12	2.05
A14	7	0.91	0.23	2.02	0.82	0.22	1.92
	90	0.88	0.23	1.87	0.83	0.22	1.62
	180	0.89	0.24	1.58	0.77	0.21	1.38
	360	0.91	0.22	1.52	0.81	0.22	1.42
A17	7	0.91	0.33	1.76	0.78	0.34	1.80
	90	0.88	0.32	1.34	0.81	0.29	1.54
	180	0.89	0.30	1.27	0.80	0.27	1.24
	360	0.89	0.33	1.28	0.79	0.29	1.29

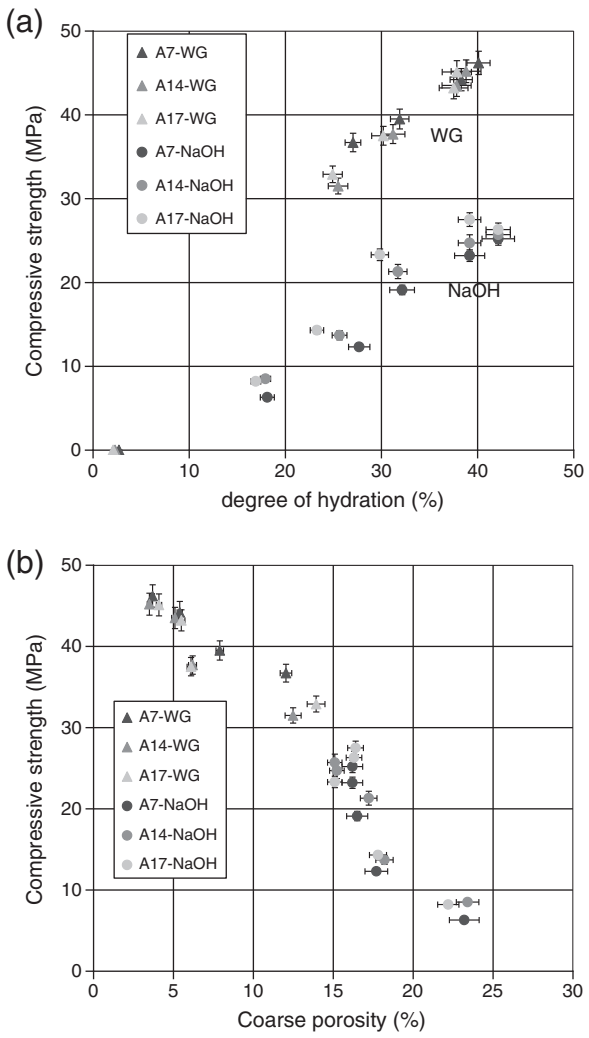

Fig. 12. Compressive strength vs. (a) degree of hydration and (b) coarse porosity of the different slags.

slags [2] or Portland cement — slag blends [57], other hydrates are formed, and the presence of additional Al_2O_3 is observed to increase compressive strength [2,57], probably due to the formation of more ettringite.

Acknowledgements

The authors would like to thank D. Rentsch (Empa, Laboratory for Functional Polymers) for his support during the NMR experiments and B. Ingold for the preparation of the polished samples for the SEM studies.

Table 8
Coarse porosity (0.05–5 μm) measured by SEM-IA (volume percent ±1%).

Activator	NaOH			WG		
Slag	A7	A14	A17	A7	A14	A17
1 day	22.2	22.4	23.2	n.m.	n.m.	n.m.
7 days	17.7	18.2	17.8	12.0	12.5	13.9
28 days	16.5	17.2	15.1	7.9	6.2	6.1
90 days	16.2	15.2	16.4	5.4	5.1	5.5
180 days	15.8	15.1	15.4	3.7	3.5	4.1
360 days	15.5	15.3	15.2	3.4	3.6	3.9

n.m.: not measured due to low degree of hydration.

References

[1] S. Caijun, L. Yinyu, Investigation on some factors affecting the characteristics of alkali-phosphorus slag cement, Cem. Concr. Res. 19 (4) (1989) 527–533.
[2] A. Gruskovnjak, B. Lothenbach, F. Winnefeld, R. Figi, S.C. Ko, M. Adler, U. Mäder, Hydration mechanisms of super sulphated slag cement, Cem. Concr. Res. 38 (7) (2008) 983–992.
[3] H.F.W. Taylor, Cement Chemistry, Thomas Telford Publishing, London, 1997.
[4] A. Gruskovnjak, B. Lothenbach, L. Holzer, R. Figi, F. Winnefeld, Hydration of alkali-activated slag: comparison with ordinary Portland cement, Adv. Cem. Res. 18 (3) (2006) 119–128.
[5] I.G. Richardson, The calcium silicate hydrates, Cem. Concr. Res. 38 (2) (2008) 137–158.
[6] S.-D. Wang, K.L. Scrivener, Hydration products of alkali activated slag cement, Cem. Concr. Res. 25 (3) (1995) 561–571.
[7] C.K. Yip, G.C. Lukey, J.S.J. van Deventer, The coexistence of geopolymeric gel and calcium silicate hydrate at the early stage of alkaline activation, Cem. Concr. Res. 35 (9) (2005) 1688–1697.
[8] D.M. Roy, Alkali-activated cements opportunities and challenges, Cem. Concr. Res. 29 (2) (1999) 249–254.
[9] F. Puertas, A. Fernández-Jiménez, Mineralogical and microstructural characterisation of alkali-activated fly ash/slag pastes, Cem. Concr. Compos. 25 (3) (2003) 287–292.
[10] M. Ben Haha, B. Lothenbach, G. Le Saout, F. Winnefeld, Influence of slag chemistry on the hydration of alkali-activated blast-furnace slag — part I: effect of MgO, Cem. Concr. Res. 41 (9) (2011) 955–963.
[11] A. Sakulich, E. Anderson, C. Schauer, M. Barsoum, Influence of Si:Al ratio on the microstructural and mechanical properties of a fine-limestone aggregate alkali-activated slag concrete, Mater. Struct. 43 (7) (2010) 1025–1035.
[12] R.L. Snyder, D.L. Bish, Quantitative Analysis, in: D.L. Bish, J.E. Post (Eds.), Modern powder diffraction, Mineralogical Society of America, 1989, pp. 101–144.
[13] M. Ben Haha, K. De Weerdt, B. Lothenbach, Quantification of the degree of reaction of fly ash, Cem. Concr. Res. 40 (11) (2010) 1620–1629.
[14] K.L. Scrivener, Backscattered electron imaging of cementitious microstructures: understanding and quantification, Cem. Concr. Compos. 26 (8) (2004) 935–945.
[15] K.L. Scrivener, H.H. Patel, P.L. Pratt, L.J. Parrott, Analysis of phases in cement paste using backscattered electron images, methanol adsorption and thermogravimetric analysis, Proceeding Material Research Society Symposium, Microstructural Development During the Hydration of Cement, 1986, pp. 67–76.
[16] D. Kulik, U. Berner, E. Curti, Modelling Geochemcial Equilibrium Partitioning with the GEMS-PSI Code, , 2004.
[17] B. Lothenbach, A. Gruskovnjak, Hydration of alkali-activated slag: thermodynamic modelling, Adv. Cem. Res. 19 (2) (2007) 81–92.
[18] B. Lothenbach, T. Matschei, G. Möschner, F.P. Glasser, Thermodynamic modelling of the effect of temperature on the hydration and porosity of Portland cement, Cem. Concr. Res. 38 (1) (2008) 1–18.
[19] D. Kulik, J. Tits, E. Wieland, Aqueous–solid solution model of strontium uptake in C–S–H phases, Geochim. Cosmochim. Acta 71 (12, Supplement 1) (2007) A530.
[20] P. Yu, R.J. Kirkpatrick, B. Poe, P.F. McMillan, X. Cong, Structure of calcium silicate hydrate (C–S–H): near-, mid-, and far-infrared spectroscopy, J. Am. Ceram. Soc. 82 (3) (1999) 742–748.
[21] I.G. Richardson, G.W. Groves, The incorporation of minor and trace elements into calcium silicate hydrates (C–S–H) gel in hardened cement pastes, Cem. Concr. Res. 23 (1993) 131–138.
[22] G. Renaudin, J. Russias, F. Leroux, F. Frizon, C. Cau-dit-Coumes, Structural characterization of C–S–H and C–A–S–H samples — part I: long-range order investigated by Rietveld analyses, J. Solid State Chem. 182 (2009) 3312–3319.
[23] N. Janes, E. Oldfield, Prediction of silicon-29 nuclear magnetic resonance chemical shifts using a group electronegativity approach: applications to silicate and aluminosilicate structures, J. Am. Chem. Soc. 107 (24) (1985) 6769–6775.
[24] K. Shimoda, Y. Tobu, K. Kanehashi, T. Nemoto, K. Saito, Total understanding of the local structures of an amorphous slag: Perspective from multi-nuclear (^{29}Si, ^{27}Al, ^{17}O, ^{25}Mg, and ^{43}Ca) solid-state NMR, J. Non-Cryst. Solids 354 (10–11) (2008) 1036–1043.
[25] Li Chao, Sun Heng Hu, L.T. Li, Glass phase structure of blast furnace slag, Adv. Mater. Res. 168–170 (2011) 3–7.
[26] Keiji Shimoda, Koji Saito, Detailed structure elucidation of the blast furnace slag by molecular dynamics simulation, Iron Steel Inst. Jpn. Int. 47 (9) (2007) 1275–1279.
[27] F. Puertas, M. Palacios, H. Manzano, J.S. Dolado, A. Rico, J. Rodriguez, A model for C–A–S–H gel formed in alkali-activated slag cements, J. Eur. Ceram. Soc. 31 (12) (2011) 2043–2056.
[28] M. Ben Haha, G. Le Saout, B. Lothenbach, F. Winnefeld, Influence of activator type on hydration kinetics, hydrate assemblage and microstructural development of alkali activated blast-furnace slags, Cem. Concr. Res. 41 (3) (2011) 301–310.
[29] A.R. Brough, A. Atkinson, Sodium silicate-based, alkali-activated slag mortars: part I. Strength, hydration and microstructure, Cem. Concr. Res. 32 (6) (2002) 865–879.
[30] J.I. Escalante-Garcia, A.F. Fuentes, A. Gorokhovsky, P.E. Fraire-Luna, G. Mendoza-Suarez, Hydration products and reactivity of blast-furnace slag activated by various alkalis, J. Am. Ceram. Soc. 86 (12) (2003) 2148–2153.
[31] A. Fernández-Jiménez, J.G. Palomo, F. Puertas, Alkali-activated slag mortars: mechanical strength behaviour, Cem. Concr. Res. 29 (8) (1999) 1313–1321.
[32] A. Fernandez-Jimenez, F. Puertas, Effect of activator mix on the hydration and strength behaviour of alkali-activated slag cements, Adv. Cem. Res. 15 (3) (2003) 129–136.

[33] C. Shi, R.L. Day, A calorimetric study of early hydration of alkali-slag cements, Cem. Concr. Res. 25 (6) (1995) 1333–1346.
[34] A. Gruskovnjak, B. Lothenbach, F. Winnefeld, B. Münch, R. Figi, S. Ko, M. Adler, U. Mäder, Quantification of hydration phases in supersulphated cements: review and new approaches, Adv. Cem. Res. (in press), doi:10.1680/adcr.2011.23.1.1.
[35] G. Le Saout, M. Ben Haha, F. Winnefeld, B. Lothenbach, Hydration degree of alkali activated slags: a 29Si NMR study, J. Am. Ceram. Soc. (in press), doi:10.1111/j.1551-2916.2011.04828.x.
[36] E.H. Oelkers, General kinetic description of multioxide silicate mineral and glass dissolution, Geochim. Cosmochim. Acta 65 (21) (2001) 3703–3719.
[37] S.A. Welch, W.J. Ullman, Feldspar dissolution in acidic and organic solutions: compositional and pH dependence of dissolution rate, Geochim. Cosmochim. Acta 60 (16) (1996) 2939–2948.
[38] R.K. Iler, Effect of adsorbed alumina on the solubility of amorphous silica in water, J. Colloid Interface Sci. 43 (2) (1973) 399–408.
[39] E.H. Oelkers, S.R. Gislason, The mechanism, rates and consequences of basaltic glass dissolution: I. An experimental study of the dissolution rates of basaltic glass as a function of aqueous Al, Si and oxalic acid concentration at 25 °C and pH = 3 and 11, Geochim. Cosmochim. Acta 65 (21) (2001) 3671–3681.
[40] B.R. Bickmore, K.L. Nagy, A.K. Gray, A.R. Brinkerhoff, The effect of $Al(OH)_4^-$ on the dissolution rate of quartz, Geochim. Cosmochim. Acta 70 (2) (2006) 290–305.
[41] M. Ben Haha, G. Le Saout, B. Lothenbach, F. Winnefeld, Study on the effect of Al_2O_3 on the hydration of slag systems using different alkaline activators, Empa Dübendorf, Switzerland, 2010.
[42] G. Renaudin, J. Russias, F. Leroux, F. Frizon, C. Cau-dit-Coumes, Structural characterization of C–S–H and C–A–S–H samples—part I: long-range order investigated by Rietveld analyses, J. Solid State Chem. 182 (12) (2009) 3312–3319.
[43] E. Kanezaki, Thermal behavior of the hydrotalcite-like layered structure of Mg and Al-layered double hydroxides with interlayer carbonate by means of in situ powder HTXRD and DTA/TG, Solid State Ionics 106 (3–4) (1998) 279–284.
[44] K. Rozov, U. Berner, C. Taviot-Gueho, F. Leroux, G. Renaudin, D. Kulik, L.W. Diamond, Synthesis and characterization of the LDH hydrotalcite–pyroaurite solid-solution series, Cem. Concr. Res. 40 (8) (2010) 1248–1254.
[45] S.-D. Wang, K.L. Scrivener, ^{29}Si and ^{27}Al NMR study of alkali-activated slag, Cem. Concr. Res. 33 (5) (2003) 769–774.
[46] D.S. Klimesch, A.S. Ray, Effect of quartz content on the nature of Al-substituted 11 Å tobermorite in hydrothermally treated $CaO–Al_2O_3–SiO_2–H_2O$ systems, Adv. Cem. Res. 11 (1999) 179–187.
[47] J. Schneider, M.A. Cincotto, H. Panepucci, 29Si and 27Al high-resolution NMR characterization of calcium silicate hydrate phases in activated blast-furnace slag pastes, Cem. Concr. Res. 31 (7) (2001) 993–1001.
[48] I.G. Richardson, A.R. Brough, R. Brydson, G.W. Groves, C.M. Dobson, Location of aluminum in substituted calcium silicate hydrate (C–S–H) gels as determined by ^{29}Si and ^{27}Al NMR and EELS, J. Am. Ceram. Soc. 76 (9) (1993) 2285–2288.
[49] S.D. Wang, Alkali-activated slag: hydration process and development of microstructure, Adv. Cem. Res. 12 (4) (2000) 163–172.
[50] D. Wan, H. Liu, X. Zhao, J. Qu, S. Xiao, Y. Hou, Role of the Mg/Al atomic ratio in hydrotalcite-supported Pd/Sn catalysts for nitrate adsorption and hydrogenation reduction, J. Colloid Interface Sci. 332 (1) (2009) 151–157.
[51] F. Puertas, A. Fernández-Jiménez, M.T. Blanco-Varela, Pore solution in alkali-activated slag cement pastes. Relation to the composition and structure of calcium silicate hydrate, Cem. Concr. Res. 34 (1) (2004) 139–148.
[52] S.J. Song, H.M. Jennings, Pore solution chemistry of alkali-activated ground granulated blast-furnace slag, Cem. Concr. Res. 29 (2) (1999) 159–170.
[53] R. Rinaldi, M. Sacerdoti, E. Passaglia, Strätlingite: crystal structure, chemistry, and a reexamination of its polytype vertumnite, Eur. J. Mineral. 2 (1990) 841–849.
[54] G. Mascolo, O. Marino, A new synthesis and characterization of magnesium-aluminium hydroxides, Mineral. Mag. 43 (1980) 619–621.
[55] E. Bonaccorsi, S. Merlino, A.R. Kampf, The crystal structure of tobermorite 14 A (Plombierite), a C–S–H phase, J. Am. Ceram. Soc. 88 (3) (2005) 505–512.
[56] A. Fernández-Jiménez, F. Puertas, Setting of alkali-activated slag cement: influence of activator nature, Adv. Cem. Res. 13 (2001) 115–121.
[57] W. Wassing, Relationship between the chemical reactivity of granulated blastfurnace slags and the mortar standard compressive strength of the blastfurnace cements produced from them, Cem. Int. 1 (5) (2003) 95–109.
[58] H.M. Jennings, A model for the microstructure of calcium silicate hydrate in cement paste, Cem. Concr. Res. 30 (2000) 101–116.